AIAA JOURNAL
Vol. 39, No. 1, January 2001

Aerodynamic Measurements of Regular Depression Roughness

M. J. Baumann* and R. J. Kind†
Carleton University, Ottawa, Ontario K1S 5B6, Canada

Three plates roughened with regular arrays of cylindrical and hemispherical depressions were tested in a wind tunnel to gain insight into the aerodynamic effects of depression roughness. The term depression roughness refers to configurations where the roughness elements are depressions whose plan area constitutes less than about one-third of the total surface area. The effects of the three depression-roughness configurations on law-of-the-wall parameters were determined. They were found to be much less than that of protrusion roughness of corresponding cross section. Hemispherical depressions produced greater increases in skin friction than cylindrical depressions of the same diameter and depth. Flow development along surfaces with depression roughness can be computed using the same methods used for protrusion roughness, provided that an equivalent protrusion height can be established for the depressions.

Nomenclature

A, B	=	constants in logarithmic law; Eqs. (1–3)
A_s, A_{xc}	=	plate area associated with each depression and depression cross-sectional area
C	=	roughness constant; see Eqs. (2) and (3)
C_f	=	skin-friction coefficient, $\tau_w/0.5\rho U^2$
d	=	diameter of depressions
H	=	boundary-layer shape factor
h	=	depth of depressions
k, k_s, k_{eq}	=	roughness element height, standard sand roughness height, and equivalent-protrusion height
U	=	freestream velocity
u, u^*	=	streamwise velocity in boundary layer and shear velocity $(\tau_w/\rho)^{0.5}$
x	=	distance from leading edge of plate
y	=	height above surface of plate
Δu	=	log-law intercept shift; see Eq. (2)
δ	=	boundary-layer thickness
θ	=	boundary-layer momentum thickness
ν	=	kinematic viscosity of fluid
ρ	=	fluid density
τ_w	=	shear stress in the fluid at $y = 0$

Introduction

SURFACE roughness can seriously degrade the aerodynamic performance of airfoils, wings, and turbomachinery blading. The roughness can take the form of protrusions, for example, dirt, bugs, frost, or ice deposits, or depressions, for example, corrosion pits. Protrusion roughness has been the subject of numerous investigations, for example, see Refs. 1–5. On the other hand, there are almost no data available for depression roughness, that is, where the roughness elements are depressions whose plan area constitutes less than about one-third of the total surface area. Kithcart and Klett[6] present average skin-friction data for surfaces with arrays of hemispherical depressions but unfortunately do not give any velocity profile data. Choi and Fujisawa[7] discuss depression roughness in qualitative terms. This paper presents data for three surfaces with regular arrays of cylindrical and hemispherical depressions and discusses how this type of roughness can be characterized for computational purposes.

Received 10 December 1999; revision received 24 May 2000; accepted for publication 24 May 2000.

*Graduate Student, Department of Mechanical and Aerospace Engineering.
†Professor, Department of Mechanical and Aerospace Engineering. Associate Fellow AIAA.

Background

The effects of roughness on aerodynamic performance can be predicted if the viscous flow over the body can be computed. Two fundamentally different approaches, the correlation approach and the discrete-element approach, are available for dealing with the roughness.

The correlation approach modifies the law of the wall or the turbulence model in the near-wall region. This requires characterization of the roughness in terms of its standard-sand height k_s or, equivalently, in terms of the shift that it produces in the logarithmic law-of-the-wall intercept. For smooth or rough walls the logarithmic portion of the law of the wall can be written as[8]

$$u/u^* = A\ln(yu^*/\nu) + B - \Delta u/u^* \tag{1}$$

The last term is an intercept shift caused by the roughness; for fully rough flow it takes the form[8]

$$\Delta u/u^* = A\ln(ku^*/\nu) + C \tag{2}$$

Equation (1) then becomes

$$u/u^* = A\ln(y/k) + B - C \tag{3}$$

Here, u is the flow velocity at height y above the wall, u^* is the shear velocity, k is the actual height of the roughness elements, and A and B are empirical constants whose values, $1/0.41$ and 5.0, respectively, have been established from smooth wall experiments.[9] Provided that the flow is indeed fully rough, C has a constant value for any particular roughness configuration and can be considered to characterize the roughness. For example, for standard-sand[1] roughness, C has a value of about -4, as shown by Grigson's[10] reanalysis of Nikuradse's data.[1] Empirical correlations are necessary to relate C to the roughness configuration. If the governing differential equations are to be integrated right from the wall, the turbulence model is modified such that the velocity distribution obtained by integration satisfies Eq. (3) in the near-wall region (see, for example, Refs. 11 and 12).

The discrete-element approach has been successfully developed by Taylor et al.[13] In their work, the flow-blockage and drag effects of the roughness elements are directly included in the partial differential equations of continuity and streamwise momentum. The equations are integrated right from the wall, and the turbulence model is not modified from the smooth-wall version. The roughness is, thus, modeled directly. Nevertheless, the discrete-element approach still requires a correlation for the aerodynamic drag of the roughness elements, and so empiricism is not completely avoided.

The present experimental results are analyzed and presented mainly in the context of the logarithmic law of the wall [Eqs. (1–3)]. That is, boundary-layer velocity profiles measured on the rough surfaces are used to determine skin-friction coefficients C_f as well as $\Delta u/u^*$ and C. Some computations were also carried out using the

Table 1 Roughness and boundary-layer parameters

						$x = 1.02$ m							
Plate	d, mm	h, mm	A_s/A_{xc}	θ, mm	H	$C_{f\,mom}$	$C_{f\,defect}$	$C_{f\,Clauser}$	$\Delta u/u^*$	k_s, mm	k_{eq}, mm	k_{eq}/h	C
Smooth	——	——	——	2.55	1.39	0.00275	0.00275	0.00275	0	——	——	——	——
1 (cylinders)	6.35	3.175	10	2.65	1.40	0.00416	0.00415	——	5.6 ± 0.2	0.39	0.72	0.23	−5.5
2 (hemispheres)	6.35	3.175	12.7	3.1	1.45	0.00458	0.00460	——	$6.9 \pm {}^{0.1}_{0}$	0.62	0.90	0.28	−4.9
3 (cylinders)	6.35	3.175	100	2.5	1.40	0.00291	0.00290	——	$0.4 \pm {}^{0}_{0.1}$	0.05	0.60	0.19	——

discrete-element approach, to aid in interpreting and extending the applicability of the results.

Experiments and Data Analysis

The experiments comprised measurements of the velocity profiles at five stations along each of three flat PVC plastic plates into which arrays of small depressions had been milled using a computer numerically controlled milling machine. The plates were 0.76 m wide × 1.83 m long, and the arrays of depressions extended over the entire surface. Plates 1 and 3 had cylindrical depressions of diameter $d = 6.35$ mm (1/4 in.) and depth $h = 3.175$ mm (1/8 in.). Plate 2 had 6.35-mm-diam × 3.175-mm-deep hemispherical depressions. The depressions were sharp edged and free of burrs. Both the spanwise spacing between depressions in each row and the streamwise spacing between rows were 14.20 mm, center to center, for plates 1 and 2 and 44.91 mm for plate 3. Successive rows were staggered. Depression positions and depths were accurate within ±0.03 mm. The roughness spacing parameter A_s/A_{xc} thus had values of 10, 12.7, and 100 for plates 1, 2, and 3, respectively.

The experimental and data analysis methods were the same as those described by Kind and Lawrysyn.[14] In brief, the rough plates covered the 0.76-m-wide by 1.83-m-long test-section floor of a low-speed wind tunnel. Test-section height was 0.5 m. A smooth plate was also tested to verify experimental techniques. The freestream wind speed U was about 50 m/s for all tests, and the streamwise pressure gradient was essentially zero. Reynolds numbers based on plate length and on boundary-layer momentum thickness at $x = 1$ m were about 5.5×10^6 and 7.9×10^3 or higher, respectively. A flattened pitot tube was traversed normal to the plate at axial stations $x = 0.31$, 0.67, 1.02, 1.37, and 1.72 m from the leading edge of the plate, along the plate centerline. The exterior mouth height of the pitot tube was 0.5 mm. Static pressures on the test-section ceiling were measured and used as a reference to determine dynamic pressures. Velocity profiles measured 0.15 m to left and right of the centerline were virtually identical to the centerline profiles, indicating good two dimensionality of the flow.

As described in Ref. 14, skin-friction coefficients C_f were determined in two ways, first by using the two-dimensional momentum integral equation and second by plotting the velocity profile data in the form u/U vs y/δ and comparing with the velocity-defect law for zero-pressure-gradient boundary layers. For the smooth plate C_f was also determined by the conventional Clauser plotting technique.[15] The pressure-gradient term was included in the momentum integral equation and was found to be negligible. In all cases, the C_f values determined by the various methods were in excellent agreement. This supports both the validity of the techniques and the two dimensionality of the flow.

Results for C_f and other boundary-layer parameters are listed in Table 1. Only values at the middle measuring station, $x = 1.02$ m, are listed because there was only slight variation along the flow, associated with development of the boundary layer. Based on repeatability checks and on comparison of C_f values determined by independent methods, uncertainties for θ, H, C_f, $\Delta u/u^*$, k_s, k_{eq}, k_{eq}/h, and C are estimated at ±0.1 mm, ±0.1, ±0.00005, ±0.1, ±10%, ±2%, ±3%, and ±0.2, respectively. In addition there is a bias error on k_s, dependent on the value chosen for C of standard-sand roughness.

Because $(u^*/U)^2 = C_f/2$, once C_f values were determined, the velocity profile data could be plotted in the form u/u^* vs yu^*/ν. The intercept shift, $\Delta u/u^*$, of Eq. (1) could then be read directly off the plots. Figure 1 illustrates the procedure for a typical velocity profile. Ideally $\Delta u/u^*$ should have the same value at all five measurement stations along each plate because the roughness configuration is uniform. In fact, there was a small variation and the values listed in Table 1 are the averages for stations 2–5, station 1 being excluded because it was near the leading edge of the rough plates and the flow may not have been completely in equilibrium. Upper and lower bounds of the variation are indicated. Once $\Delta u/u^*$ values are determined, the equivalent standard-sand[l] roughness height k_s can be found using Eq. (2). Table 1 lists k_s values determined using Grigson's[10] value of -4 for C. The value of k_s for plate 3 is only an approximate measure because, as discussed later, the flow is not fully rough for this case.

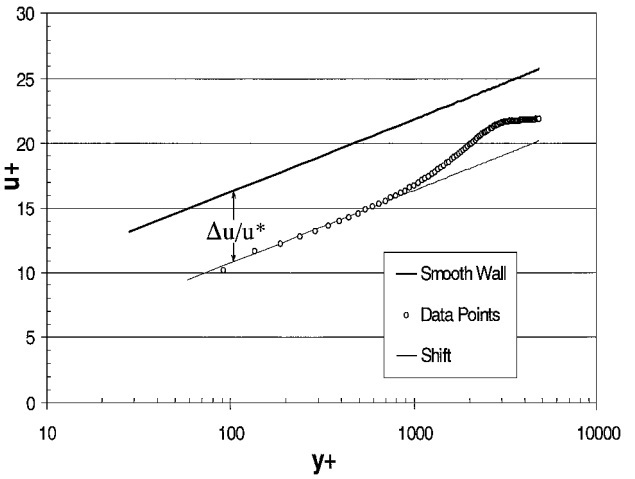

Fig. 1 Method for determining log-law intercept shift (plate 1, $x = 1.02$ m).

The objective of the experiments was to characterize each of the three tested roughness configurations in terms of aerodynamic parameters that could be used in computational models. Both the correlation and the discrete-element approaches have been developed only for protrusion roughness. To assess how the present results for depression roughness fit in with those available for protrusion roughness, it is useful to determine an equivalent-protrusion height k_{eq} for the depression roughness elements. This was done by doing computations with the discrete-element model.

Discrete-Element Computations

The strategy was to compute boundary-layer development over surfaces roughened by cylindrical protrusions having the same diameter and distributed over the surface in the same way as the actual depressions, but having a height k_{eq} such that the flow development over the hypothetical surface was the same as that over the actual surface.

The computations were carried out using TSL, a Navier–Stokes code developed for solution of thin two-dimensional shear layers.[16] The equations are in primitive variable form and are parabolized, allowing use of a fast streamwise marching algorithm. The code has been verified against available laminar and turbulent flow solutions. The discrete element roughness model of Taylor et al.[13] was implemented in the code,[17] and the Baldwin–Lomax[18] turbulence model was used for the present computations.

Computations with various values of k_{eq} were carried out for each of the three rough plates. The starting velocity profiles were those measured at $x = 0.31$ m. For each plate a value of k_{eq} was found

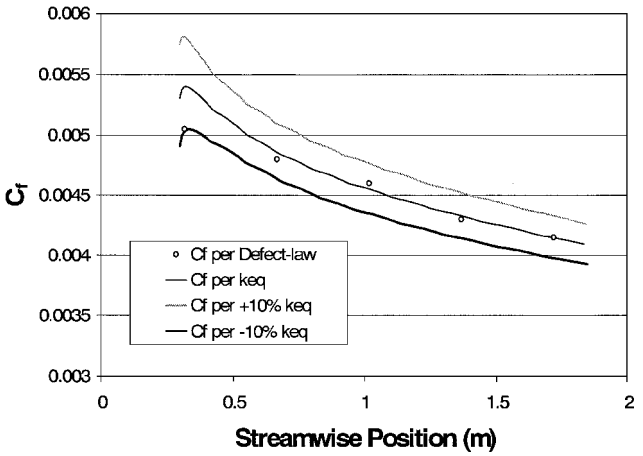

Fig. 2 Typical comparison between discrete-element calculations and experiment (plate 2).

that gave very good agreement between measured and computed boundary-layer parameters at measurement stations 2–5. Figure 2 shows typical results. The values found for k_{eq} are listed in Table 1.

The values of $k_s u^*/\nu$ were 51, 87, and approximately 6 for plates 1, 2, and 3, respectively. The values for plates 1 and 2 are at or above the value of about 50, commonly accepted as the lower limit for fully rough flow. Thus, C is expected to be a constant that characterizes the roughness configuration for each of plates 1 and 2, and the values can be found from Eq. (2), using k_{eq} for k and the experimental values for $\Delta u/u^*$. The values of C, thus determined, are included in Table 1. No value is given for C for plate 3 because the value of about 6 for $k_s u^*/\nu$ is far below the limit for fully rough flow and C cannot be expected to have a constant value for this case.[8] The shear stress on the surface between depressions constitutes an important fraction of the drag on plate 3, so that in this case C depends on Reynolds number as well as on the roughness configuration.

Discussion

The k_{eq} values in Table 1 are much less than the depression depth h. This is to be expected because flow skimming over a hole will tend to be retarded much less than flow impinging onto a protrusion of corresponding diameter and height. For the cylindrical depressions, the ratio k_{eq}/h has a value of about 0.2, which implies that the drag of the cylindrical depressions is about 20% that of corresponding protrusions. This corresponds closely with a drag ratio estimate, 0.19, obtained by using low Mach number data for the drag of isolated cylindrical depressions[19] and protrusions[20] having $h/d = 0.5$. This finding enhances the credibility of the present results and also indicates that for the present range of A_s/A_{xc} the flow over each depression in the roughness array is essentially the same as that over an isolated depression.

Comparison of the k_{eq} value for plate 2 (hemispherical depressions, $A_s/A_{xc} = 12.7$) with that for plate 1 (cylindrical depressions, $A_s/A_{xc} = 10$) indicates that hemispherical depressions produce more drag force than cylindrical depressions of the same diameter and depth. The flow in and over depressions is known to be very complex,[19] and it is quite plausible that hemispherical depressions produce a stronger perturbation to the overall flow.

The individual depressions in plates 1 and 3 were identical (6.35-mm-diam × 3.175-mm-deep cylindrical holes). At 0.72 and 0.60 mm, respectively, the k_{eq} values found as outlined earlier are not, however, identical; in fact, they differ by about 20%, substantially more than the range of uncertainty. This implies that the drag force associated with individual depressions is somewhat different for the two plates, being larger for the plate with the denser hole pattern. This could result from a combination of higher drag force on individual depressions and higher shear stress on the surface between depressions when the depressions are more densely spaced.

If the near-wall mixing length vs y relation does not vary greatly, the higher C_f associated with denser depression spacing implies larger velocity gradients and, thus, higher velocities near the wall. Both higher drag force on individual depressions and higher surface shear stress between depressions would be consistent with this. These effects, particularly the increased surface shear stresses, would not be captured with complete correctness by the discrete-element model if the depressions are simply replaced by equivalent protrusions as was done in the present computations. It appears that some further development of the discrete-element method is required to enable it to more accurately predict the effects of depression roughness. Blockage effects and y position of the momentum sink associated with the depressions need to be represented more appropriately.

The preceding discussion indicates that there are some shortcomings in the concept of representing depression roughness effects by replacing the depressions by equivalent protrusions. Nevertheless, an order of magnitude change in the value of the spacing parameter A_s/A_{xc} results in only a 20% change in the equivalent-protrusion height k_{eq}. The equivalent-protrusion approach thus has potential for working fairly well, at least for $A_s/A_{xc} \geq 10$, provided that a correlation between depression geometry and equivalent protrusion height can be established. In the interim, the following approach could be used to compute approximate flow development over surfaces having cylindrical or hemispherical depression roughness with $h/d = 0.5$. The k_{eq}/h values could be estimated from Table 1 and used with either the discrete-element or, for fully rough cases, the correlation method. Once k_{eq}/h has been chosen, the inputs for a discrete-element computation are straightforward. To use the correlation method, an appropriate value of C or equivalent k_s must also be determined. The most straightforward approach would be to estimate a value for C from Table 1, using $\log(A_s/A_{xc})$ as an interpolation parameter. Alternately, C could be found by using $k = k_{eq}$, together with the depression diameter and distances between depressions, in the correlation of Simpson.[21] This correlation gives values for C within 1.0 of the experimental values for plates 1 and 2, an accuracy about three times better than the correlation of Waigh and Kind[22] for these two cases.

The drag coefficient of cylindrical depressions varies strongly with their depth-to-diameter ratio, h/d (Ref. 19). Indeed, the data in Ref. 19 vary by a factor of almost 10 for $0.05 \leq h/d \leq 1.5$ at subsonic Mach number. The results in Table 1 should not, therefore, be used for h/d values substantially different from 0.5 unless they are appropriately adjusted. For arrays of cylindrical depressions it may be satisfactory for some purposes to simply multiply the k_{eq}/h values of Table 1 by the ratio of drag coefficient for isolated depressions having the h/d of interest to that for $h/d = 0.5$.

Conclusions

Three plates roughened with regular arrays of cylindrical and hemispherical depressions have been tested in a wind tunnel. Equivalent roughness-element height and effect on the logarithmic portion of the law of the wall have been determined.

The effect of depression roughness is much less than that of protrusion roughness of corresponding cross section. Hemispherical depressions produced substantially more drag than cylindrical depressions of the same diameter and depth.

In the discrete-element prediction method, individual depressions can be approximately represented by protrusions of some suitable equivalent height. The equivalent height varies somewhat with depression spacing, indicating minor inconsistencies and a need for improvement of the model. Moreover, a scheme for determining equivalent height needs to be developed.

Acknowledgment

The authors gratefully acknowledge support from a Natural Sciences and Engineering Research Council of Canada Research Grant.

References

[1] Nikuradse, J., "Strömungsgesetze in Rauen Rohren," *VDI Forschungsheft*, Vol. 361, No. 4, 1933 (available in English as NACA TM 1292, 1950).

[2] Coleman, H. W., Hodge, B. K., and Taylor, R. P., "A Re-Evaluation of Schlichting's Surface Roughness Experiment," *Journal of Fluids Engineering*, Vol. 106, March 1984, pp. 60–65.

[3]Dvorak, F. A., "Calculation of Turbulent Boundary Layers on Rough Surfaces in Pressure Gradient," *AIAA Journal*, Vol. 7, No. 9, 1969, pp. 1752–1759.

[4]Scraggs, W. F., Taylor, R. P., and Coleman, H. W., "Measurement and Prediction of Rough Wall Effects on Friction Factor—Uniform Roughness Results," *Journal of Fluids Engineering*, Vol. 110, Dec. 1988, pp. 385–391.

[5]Raupach, M. R., Antonia, R. A., and Rajagopalan, S., "Rough-Wall Turbulent Boundary Layers," *Applied Mechanics Reviews*, Vol. 44, No. 1, 1991, pp. 1–25.

[6]Kithcart, M. E., and Klett, D. E., "Heat Transfer and Skin Friction Comparison of Dimpled Versus Protrusion Roughness," *Journal of Enhanced Heat Transfer*, Vol. 3, No. 4, 1996, pp. 273–280.

[7]Choi, K. S., and Fujisawa, N., "Possibility of Drag Reduction Using d-Type Roughness," *Applied Scientific Research*, Vol. 50, 1993, pp. 315–324.

[8]Clauser, F. H., "The Turbulent Boundary Layer," *Advances in Applied Mechanics*, Vol. 4, 1956, pp. 1–51.

[9]White, F. M., *Viscous Fluid Flow*, 2nd ed., McGraw–Hill, New York, 1991, Chap. 6.

[10]Grigson, G. W. B., "Nikuradse's Experiment," *AIAA Journal*, Vol. 22, No. 7, 1984, pp. 1000, 1001.

[11]Cebeci, T., and Chang, K. C., "Calculation of Incompressible Rough-Wall Boundary-Layer Flows," *AIAA Journal*, Vol. 16, No. 7, 1978, pp. 730–735.

[12]Zhang, H., Faghri, M., and White, F. M., "A New Low-Reynolds-Number k–ε Model for Turbulent Flow Over Smooth and Rough Surfaces," *Journal of Fluids Engineering*, Vol. 118, June 1996, pp. 255–259.

[13]Taylor, R. P., Coleman, H. W., and Hodge, B. K., "Prediction of Turbulent Rough-Wall Skin Friction Using a Discrete Element Approach," *Journal of Fluids Engiineering*, Vol. 107, No. 6, 1985, pp. 251–256.

[14]Kind, R. J., and Lawrysyn, M. A., "Aerodynamic Characteristics of Hoar Frost Roughness," *AIAA Journal*, Vol. 30, No. 7, 1992, pp. 1703–1707.

[15]Clauser, F. H., "Turbulent Boundary Layers in Adverse Pressure Gradients," *Journal of the Aeronautical Sciences*, Vol. 21, No. 2, 1954, pp. 91–108.

[16]Pajayakrit, P., "Turbulence Modelling for Curved Wall Jets Under Adverse Pressure Gradient," Ph.D. Thesis, Dept. of Mechanical and Aerospace Engineering, Carleton Univ., Ottawa, ON, Canada, July 1997.

[17]Gagné, J. F., "An Improved Method for Modelling Fully Rough Turbulent Boundary Layer Flows," M.Eng. Thesis, Dept. of Mechanical and Aerospace Engineering, Carleton Univ., Ottawa, ON, Canada, July 1998.

[18]Baldwin, B., and Lomax, H., "Thin-Layer Approximation and Algebraic Model for Separated Turbulent Flows," AIAA Paper 78-257, 1978.

[19]Gaudet, L., and Winter, K. G., "Measurements of the Drag of Some Characteristic Aircraft Excresences Immersed in Turbulent Boundary Layers," CP-124, AGARD, 1973.

[20]Hoerner, S. F., *Fluid-Dynamic Drag*, Hoerner Fluid Dynamics, Brick Town, NJ, 1965, pp. 5–8.

[21]Simpson, R. L., "A Generalized Correlation of Roughness Density Effects on the Turbulent Boundary Layer," *AIAA Journal*, Vol. 11, No. 2, 1973, pp. 242–244.

[22]Waigh, D. R., and Kind, R. J., "Improved Aerodynamic Characterization of Regular Three-Dimensional Roughness," *AIAA Journal*, Vol. 36, No. 6, 1998, pp. 1117–1119.

M. Samimy
Associate Editor